# Ultrasensitive Detection of MCF-7 Cells with a Carbon Nanotube-Based Optoelectronic-Pulse Sensor Framework

Sophia S. Y. Chan, Denise Lee, Maria Prisca Meivita, Lunna Li, Yaw Sing Tan, Natasa Bajalovic,* and Desmond K. Loke*

Read Online

ACCESS | Metrics & More | Article Recommendations | Supporting Information

**ABSTRACT:** Biosensors are of vital significance for healthcare by supporting the management of infectious diseases for preventing pandemics and the diagnosis of life-threatening conditions such as cancer. However, the advancement of the field can be limited by low sensing accuracy. Here, we altered the bioelectrical signatures of the cells using carbon nanotubes (CNTs) via structural loosening effects. Using an alternating current (AC) pulse under light irradiation, we developed a photo-assisted AC pulse sensor based on CNTs to differentiate between healthy breast epithelial cells (MCF-10A) and luminal breast cancer cells (MCF-7) within a heterogeneous cell population. We observed a previously undemonstrated increase in current contrast for MCF-7 cells with CNTs compared to MCF-10A cells with CNTs under light exposure. Moreover, we obtained a detection limit of $\sim 1.5 \times 10^3$ cells below a baseline of $\sim 1 \times 10^4$ cells for existing electrical-based sensors for an adherent, heterogeneous cell population. All-atom molecular dynamics (MD) simulations reveal that interactions between the embedded CNT and cancer cell membranes result in a less rigid lipid bilayer structure, which can facilitate CNT translocation for enhancing current. This as-yet unconsidered cancer cell-specific method based on the unique optoelectrical properties of CNTs represents a strategy for unlocking the detection of a small population of cancer cells and provides a promising route for the early diagnosis, monitoring, and staging of cancer.
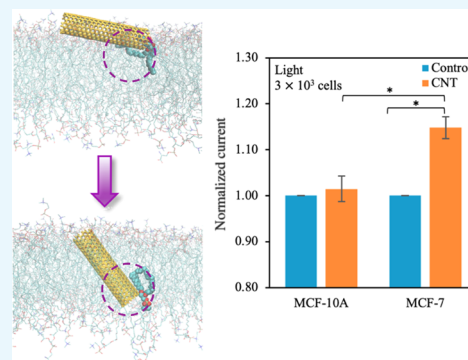
## INTRODUCTION

Biosensors are capable of detecting chemical compounds and biomolecules and have been harnessed in multiple fields such as agriculture, food safety, medical testing, and nanobiotechnology. The detection of certain biomarkers is critical in diagnosing and monitoring diseases; for example, the recent Covid-19 pandemic has created an increasing demand for new types of biosensors.[1] New biosensor systems designed to detect appropriate biomarkers are required for diagnosing diseases quickly and easily, often in remote and inaccessible locations. Cancer-relevant biosensors require a suitable biomarker to detect small populations of cancer cells in a heterogeneous cell population for early diagnosis. For example, cancer-based biosensors have been designed to detect mucin-1 (MUC-1), a commonly overexpressed breast cancer biomarker.[2−5] MUC-1 aptamers (short oligonucleotide sequences) are utilized to functionalize probes that can be detected using traditional methods such as fluorescent imaging[2,3] and quantitative real-time polymerase chain reaction (PCR).[4,5] However, these methods can be limited for early diagnosis because they tend to be labor-intensive, require additional preparation steps, and may have long waiting times.[6] New sensors are urgently needed to detect a small population of cancer cells for clinical disease diagnosis.

Currently, breast cancer is diagnosed via biopsies of suspicious breast abnormalities.[7] These methods include fine-needle aspiration (FNA), vacuum-assisted biopsy, core needle biopsy, and surgical excision biopsies.[7−9] Biopsies involve removing concerned tissues and analyzing them under a microscope.[10] However, with recent advancements in technology, it is of vital significance to identify highly accurate sensing strategies that can differentiate between normal and malignant cells. Bioelectrical signatures are ideal candidates for detecting cancer cells as they are native to cells and could reduce additional and complex preparation steps. During cancer development, a healthy cell undergoes many structural and physical changes (e.g., changes in lipid composition, membrane stiffness, etc.),[11,12] leading to observable changes in its bioelectrical properties.[13,14] Marino et al. observed depolarization (lower cell potential) of breast cancer cells in vitro compared to healthy breast epithelial cells,[15] while Qiao et al. measured a lower cell conductivity in cancer cells compared to healthy cells.[16] Thus, the native bioelectrical signature of cells is
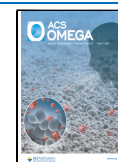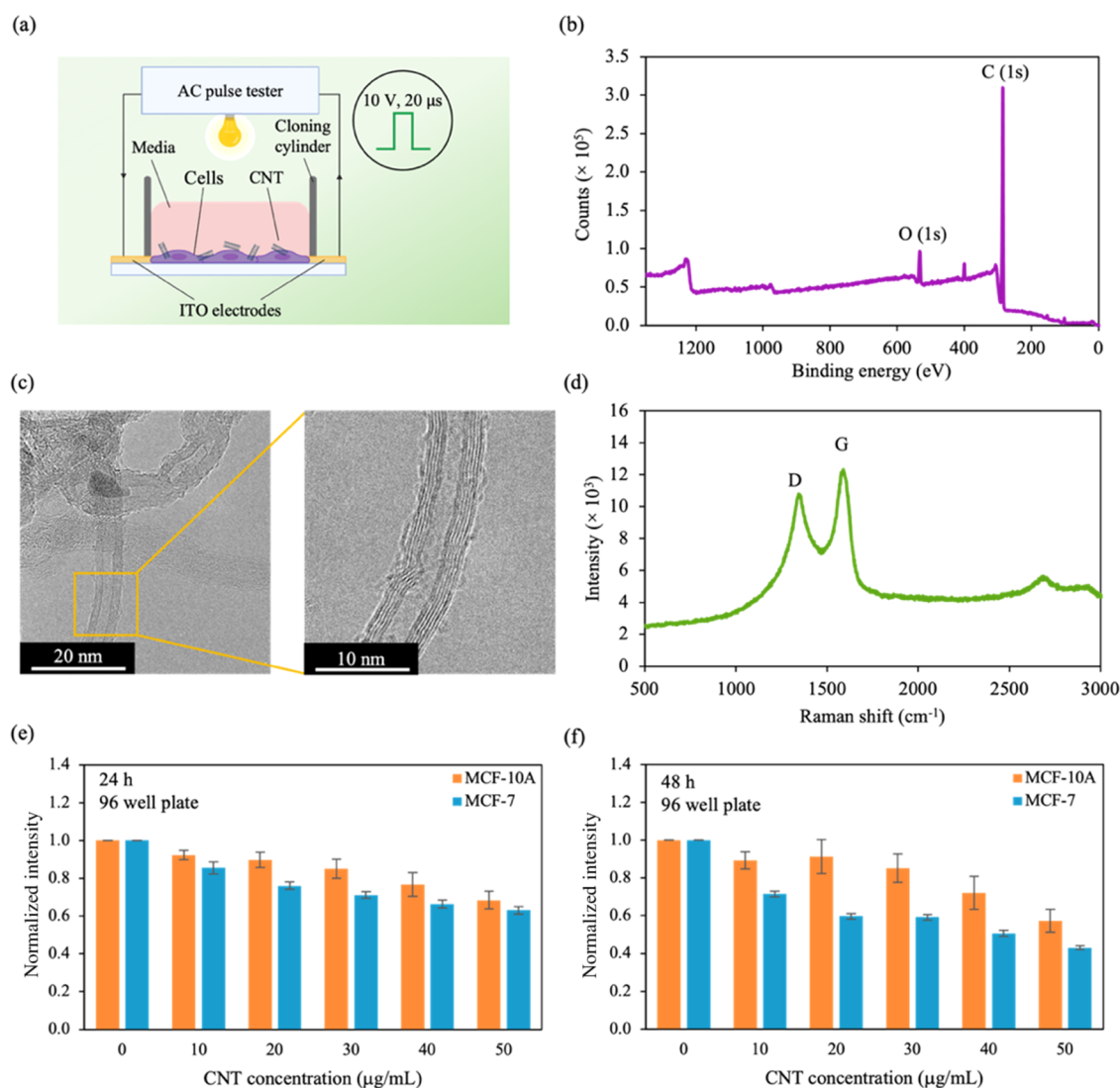
**Figure 1.** System configuration and characterization of CNT materials. (a) Schematic illustration of the testing setup. Cells were plated in the cell well: ITO electrodes on a glass substrate with a cloning cylinder secured with silicone adhesive. Cells were electrically stimulated with an AC square wave pulse (amplitude = 10 V, pulse width = 20 $\mu$s). (b) X-ray photoelectron spectroscopy (XPS) spectra of CNTs. Characteristic 1s orbital peaks for carbon (C) and oxygen (O) were observed at ∼285 and ∼532 eV, respectively. (c) Transmission electron microscopy (TEM) image of CNTs displaying well-aligned carbon atoms (left panel) and a close-up image of a CNT (right panel). (d) Raman spectra of CNTs showing peaks at ∼1344.3 and ∼1588.1 cm$^{-1}$ for the D and G bands, respectively. (e, f) Cytotoxic responses of MCF-10A (orange) and MCF-7 (blue) to different concentrations of CNTs, with incubation time of (e) 24 h and (f) 48 h. Cell viability was estimated using a WST-1 assay. Data represent the mean $\pm$ standard error of the mean (SEM), ($n = 6$ from 3 independent experiments). The statistical significance can be found in Supporting Information Table S4.

a promising biomarker to detect and distinguish cancer cells from healthy cells.

Electrical-based techniques have been investigated as a tool to detect and distinguish cancer cells from their healthy counterparts based on cell impedance or electrical conductivity because of their many advantages, such as real-time monitoring, convenience to use, simple implementation, cost-effectiveness, etc.[14,17] As tumors comprise multiple cells with important cell—cell interconnects,[18,19] it is necessary to study and detect cancer cells in an adherent population rather than in suspension. Currently, there is limited literature on the utilization of electrical-based methods to differentiate between an adherent population of healthy and cancer cells; this could be due to the large limit of detection (approximately ten thousand cells) observed for traditional electrical-based approaches.[20] Recently, various nanomaterials have been used in biosensors to reduce the limit of detection, such as nanosheets, nanowires, nanotubes,

etc.[21,22] However, few have described nanomaterials that can identify and differentiate cancer cells from their healthy counterparts using their unique cell-specific interactions. Identifying a nanomaterial with preferential interaction for one cell type over another is critical.

Carbon nanotubes (CNTs) are sheets of graphene rolled into tubes and have a hexagonal structure with free $\pi$-electrons, making them unique one-dimensional (1D) materials with excellent properties.[23,24] Similar to graphene, CNTs have a tunable band structure that contributes to their unique electrical and optical properties.[23,25] Furthermore, CNTs possess excellent photoconductive properties.[26] Due to their 1D size, CNTs have the ability to produce and separate electron—hole pairs when exposed to light, exhibiting enhanced photoconductivity with increasing light intensity.[23,27] As a result, CNTs are currently being used in optoelectronic devices, such as photoresistors, photodetectors, phototransistors, and other

devices.[23,25,28] Although the optical properties of CNTs have been studied, their application in optoelectronic sensing for cancer cells remains elusive.

Here, we altered the bioelectrical signatures of cells using CNTs with alternating current (AC) pulse under light irradiation and developed a photo-assisted AC pulse sensor based on CNTs to differentiate between MCF-10A cells and MCF-7 cells in a heterogeneous cell population. MCF-7 is a breast cancer cell line that has been intensively utilized as a model in breast cancer studies.[29,30] This method achieved a previously unobserved increased current contrast between MCF-7 cells and MCF-10A cells under light excitation compared to dark conditions. Additionally, this method detected a small population of MCF-7 cells within a heterogeneous population, with a detection limit of ∼1.5 × $10^3$ cells. This detection limit, below a baseline of ∼1 × $10^4$ cells[17] for existing electrical-based sensors, allows for sensitive detection of a small population of cancer cells for early cancer detection. All-atom molecular dynamics (MD) simulations reveal structural loosening effects in the cancer lipid bilayer system with embedded CNTs, facilitating CNT translocation through the lipid bilayer for enhancing current. Moreover, traditional fluorescent-based systems can be costly and require complex equipment for cell detection.[31,32] In this work, the system is compact, low in cost, and has easy-to-use, reusable components, which can be adopted by users with a wide range of expertise and improve user convenience and accessibility. Additionally, it is extremely challenging to create systems that can differentiate between healthy and cancer cells with an increased contrast in current, which simultaneously demonstrates low cytotoxicity of the components for reliable cancer diagnosis. The described CNT photo-assisted AC pulse system can differentiate between healthy and cancer cells with a marked contrast in current and maintain excellent biocompatibility of the cells. This proposed methodology based on the unique optoelectrical properties of CNT nanomaterials holds excellent potential for developing lab-on-chip platforms, which can be further harnessed for clinical purposes.

## ■ EXPERIMENTAL AND SIMULATION SECTION

**CNT Preparation.** CNT (1 wt %) in water (US Research Nanomaterials, US4120W) was sonicated (Elmasonic, S 130H) for ∼20 min at room temperature (RT) before material characterization and incubation with cells. CNT was drop-casted on a silicon (Si) substrate prior to transmission electron microscopy (TEM), X-ray photoelectron spectroscopy (XPS), and Raman spectroscopy. The chemical composition of CNT was analyzed using electron-dispersive X-ray spectroscopy (EDS) point analysis: C, ∼95 atom %; O, ∼5 atom %.

**Cell Culture.** Breast cancer cell line MCF-7 was cultured in Dulbecco's modified Eagle media (DMEM) (08458-45, Nacalai Tesque) containing 7% fetal bovine serum (FBS, 26140079, Gibco) and 5 mM L-glutamine (25030149, Gibco). Healthy breast epithelial cell line MCF-10A were cultured in DMEM supplemented with Ham's F12 (DMEM/F12, 11320033, Gibco) containing 10% FBS, 20 ng/mL epidermal growth factor (EGF, PHG0311L, Gibco), 0.5 μg/mL hydrocortisone (H0888-1G, Sigma), and 10 μg/mL insulin (12585014, Sigma-Aldrich). Cells were maintained in a 5% $CO_2$ environment at 37 °C and observed using an inverted light microscope with a 10× objective lens (Olympus DP22).

To test the heterogeneous cell population, a mixture of MCF-10A cells and MCF-7 cells were plated in the CNT

optoelectronic system in various populations with a total cell population of 3 × $10^3$ cells. The population of MCF-7 cells within the heterogeneous cell mixture was plated from 0 to 100% at 25% increments. Details of the cell population are presented in Supporting Information Table S1. The heterogeneous cell population was plated in MCF-10A cell media; MCF-7 cells in MCF-10A cell media grew and proliferated well after 24 and 48 h (Supporting Information Figure S1).

**System Setup.** The system comprised two left and right indium tin oxide (ITO) electrodes on a glass substrate (LaTech) with a cloning cylinder (C3983-50EA, Sigma-Aldrich) secured using a silicone adhesive (Figure 1a). The size of the gap between the electrodes was chosen to be ∼0.1 mm. Prior to cell-plating, the system was sterilized with UV light (5 min) and pure ethanol (E7023-1L, Sigma-Aldrich) (20 min) in the biosafety cabinet. The system is reusable; after detaching the cloning cylinder from the ITO substrate, both components were soaked in bleach overnight. They were then rinsed with DI water and dried in the oven before removing the silicone adhesive. After sonicating in a mixture of soap and water for ∼10 min, the cloning cylinder and substrate were rinsed in DI water and ethanol and dried in the oven before further use.

**Electrical Characterization.** MCF-10A cells and MCF-7 cells (3 × $10^3$ cells) were grown in the system ∼24 h prior to material addition. MCF-10A cells demonstrated comparable growth and proliferation after incubation without CNT (control) and with CNT within the ITO systems (Supporting Information Figure S2). After incubating the material with the cells for an additional ∼24 h, current measurements were performed using the semiconductor characterization system (Keithly 4200-SCS). A bias voltage, square wave AC pulse was applied to detect cell current (amplitude = 10 V, pulse width = 20 μs) under dark conditions. For experiments with light exposure, conditions were kept the same, and cells were pulsed under light exposure from a light-emitting diode (LED) illuminator within a microscope (eVueIII) for the duration of the measurement (∼40 μs). The LED illuminator has the specifications of LED power of ∼90 W (we define the light intensity of 100% to be 90 W). Cells were exposed to different light intensities (0, 50, and 100%) during current measurements to demonstrate light-assisted current flow (Supporting Information Figure S3). For cells in a heterogeneous cell population, cells were subjected to material addition and electrical pulses under light exposure, as mentioned above.

**Cell Viability Testing.** MCF-10A cells and MCF-7 cells (3 × $10^3$ cells) were seeded in our system and grown for 24 and 48 h prior to cell viability testing (Supporting Information Figure S1). To test for CNT cytotoxicity, MCF-10A cells and MCF-7 cells were plated in 96-well plates and cultured for ∼24 and 48 h prior to treatment. The CNT was added at a concentration ranging from 0−50 μg/mL at 10 μg/mL increments for 24 and 48 h. To demonstrate that cell viability can be maintained in different cell media for heterogeneous cell population, MCF-7 cells were plated in 96-well plates and incubated with MCF-7 and MCF-10A cell media for 24 and 48 h. Cell viability and cytotoxic effects of CNTs were determined using a WST-1 assay. After adding 10% WST-1 (Sigma-Aldrich) in media, the cells were incubated for ∼4 h. Absorbance was read at $\lambda$ = 450 nm. For WST-1 assays performed in the ITO system, cells were incubated for ∼4 h and the resultant media was transferred to a 96-well plate before reading.

**Simulation Parameterization.** An (8, 8) armchair CNT with a diameter of 1.1 nm and a length (l) of 4.5 nm was built

using the Nanotube Builder module in VMD.[33] Hydrogen atoms (H) were manually added to the open ends of the CNTs using PyMOL. Atomic charges were derived based on a short (8, 8) armchair CNT ($l$ = 0.75 nm) using the R.E.D. Server,[34] by fitting electrostatic potential (RESP) charges[35] to a molecular electrostatic potential (MEP) computed by the Gaussian 16 program[36] at the HF/6-31G* level of theory (Supporting Information Table S2).

The compositions of the healthy and cancer lipid bilayer systems were based on those used by Klähn and Zacharias,[37] and the lipid bilayers were generated using CHARMM-GUI.[38] Each lipid bilayer system was composed only of neutral dipalmitoyl-phosphatidylcholine (DOPC) and negatively charged dipalmitoylphosphatidylserine (DOPS) lipids, comprising a total of 242 lipids, 121 in each leaflet (composition found in Supporting Information Table S3). The simulation box contained 40 TIP3P water molecules per lipid and 0.15 M NaCl.[39] After the lipid bilayer was equilibrated for 50 ns, the CNT was added and the simulation was performed for 500 ns.

For the experiments, fabrication methods can be sufficient to achieve multi-walled CNTs. For the simulations, molecular dynamics simulations of the equilibrium structure and dynamics behavior of CNTs have been conducted using state-of-the-art computational techniques. However, it is possible that the computational resource is not large enough, resulting in the use of single-walled CNT.

**Simulation Details.** MD simulations were performed with GROMACS 5.0.4 using the Slipids force field for the lipids[39−42] and GAFF for the CNT.[43] The CNT was positioned perpendicular to and ~2 nm above the lipid bilayer in a simulation box ($z$ = 12 nm), which was then filled with TIP3P water molecules[44] and 0.15 M NaCl. An additional 27 sodium ions were added to the healthy lipid bilayer system, and 52 sodium ions were added to the cancer lipid bilayer to neutralize the negatively charged DOPS lipids. Each system was energy-minimized using the steepest descent algorithm (up to 2000 steps) and equilibrated using an isochoric−isothermal (NVT) ensemble for $t$ = 100 ps. The temperature of the system was maintained at $T$ = 300 K using the velocity-rescaling thermostat[45] with a 0.5 ps coupling constant. Another equilibration step was performed in the isothermal−isobaric (NPT) ensemble for $t$ = 100 ps, followed by the production run for 500 ns. The pressure was kept constant at $P$ = 1 bar by the Parrinello−Rahman barostat,[46] with a semi-isotropic pressure coupling scheme, while the temperature was kept constant using the Nosé−Hoover thermostat.[47,48] For each lipid bilayer system, two independent MD simulations were performed. Long-range electrostatic interactions were accounted for by treating the system with the particle−mesh Ewald scheme,[49,50] while a cutoff distance of 1 nm was applied to the calculation of van der Waals interactions. The LINCS algorithm was utilized to constrain all lipid and CNT bonds.[51] A time step of 2 fs was used with a Leap-Frog integrator, and coordinates of all atoms were saved every 20 ps.

**Simulation Analysis.** The average adhesion energy for the system was calculated for $t$ = 0−500 ns, using

$$\Delta E = E_{\text{total}} - (E_{\text{CNT}} + E_{\text{lipid bilayer}}) \tag{1}$$

where $E_{\text{total}}$ is the average potential energy of the entire system (CNT and lipid bilayer), $E_{\text{CNT}}$ is the average potential energy of the CNT, and $E_{\text{lipid bilayer}}$ is the average potential energy of the lipid bilayer.[52]

The number of DOPC lipids within 6 Å of the CNT at $t$ = 500 ns was calculated using $gmx\ mindist$ tool in Gromacs, and the percentage of DOPC molecules around the CNT within each lipid bilayer system was calculated via

$$\%\text{DOPC lipids} = \frac{n_{\text{CNT}}}{n_{\text{total}}} \times 100\% \tag{2}$$

where $n_{\text{CNT}}$ is the number of DOPC molecules that are within 6 Å of the CNT, and $n_{\text{total}}$ is the total number of DOPC molecules within the lipid bilayer system.

The Gromacs tool $gmx\ msd$ was utilized to determine the mean squared displacement (MSD) for the system before (0−40 ns) and after CNT interaction (last 100 ns of the simulation). The self-diffusion coefficient for each system was estimated from the MSD plots.

## ■ RESULTS

We adopted a strategy to investigate the bioelectrical signals of healthy and cancer cells with CNTs based on the CNT photo-assisted AC pulse system. The system setup, depicted in Figure 1a, comprises two 650 nm thick indium tin oxide (ITO) left and right electrodes deposited onto a glass substrate to connect the cell culture to the external circuitry. The size of the gap between the electrodes was kept constant at ~0.1 mm. The cloning cylinders were then secured with a silicone adhesive for cell storage. To differentiate between the healthy breast epithelial (MCF-10A) cells and luminal breast cancer (MCF-7) cells, the CNT was then added to the cells ~24 h before applying an electrical square wave pulse (amplitude = 10 V, pulse width = 20 μs). CNT is a unique nanomaterial with excellent photocurrent properties (it demonstrates enhanced current flow with light exposure). Because of their unique band gap structure and high carrier mobility, CNTs can harness the light energy and convert it into current by separating the electron−hole pairs (photo-current).[23,27] This exceptional property of CNTs, in combination with the unique bioelectrical signals of MCF-7 cells and their interaction with CNTs, can enhance cell-specific current signals and identify MCF-7 cells within a heterogeneous population.

Before investigating the interaction between the CNT and the cells, the chemical composition and morphology of the CNT were systematically examined. CNTs were sonicated for ~20 min prior to characterization and incubation with cells. To characterize the material, sonicated CNTs were drop-casted onto a silicon substrate. From the X-ray photoelectron spectroscopy (XPS), we observe typical peaks for CNTs. Figure 1b shows a large peak at ~285 eV corresponding to the C1s binding energy and a smaller peak at ~532 eV representing the O 1s binding energy. This suggests that the CNT might be slightly oxidized. Figure 1c shows a transmission electron microscope (TEM) image of the CNTs, in which long, entangled tube-like structures were observed. Moreover, the close-up of TEM images showed that the walls of these structures were formed by defined carbon atoms. To investigate the crystal structure and quality of the CNTs, the Raman spectra of the CNT were investigated. The Raman spectra for the CNTs showed two distinct peaks (Figure 1d). The G band (~1588.1 cm$^{-1}$) is associated with the in-plane E$_{2g}$ stretching vibration along the nanotube axis, while the defects in the CNT are represented in the D band at ~1344.3 cm$^{-1}$, which could be due to the oxidation of the CNT.

The cytotoxicity profile of the CNTs was also investigated for the MCF-10A cells and MCF-7 cells. We investigated the
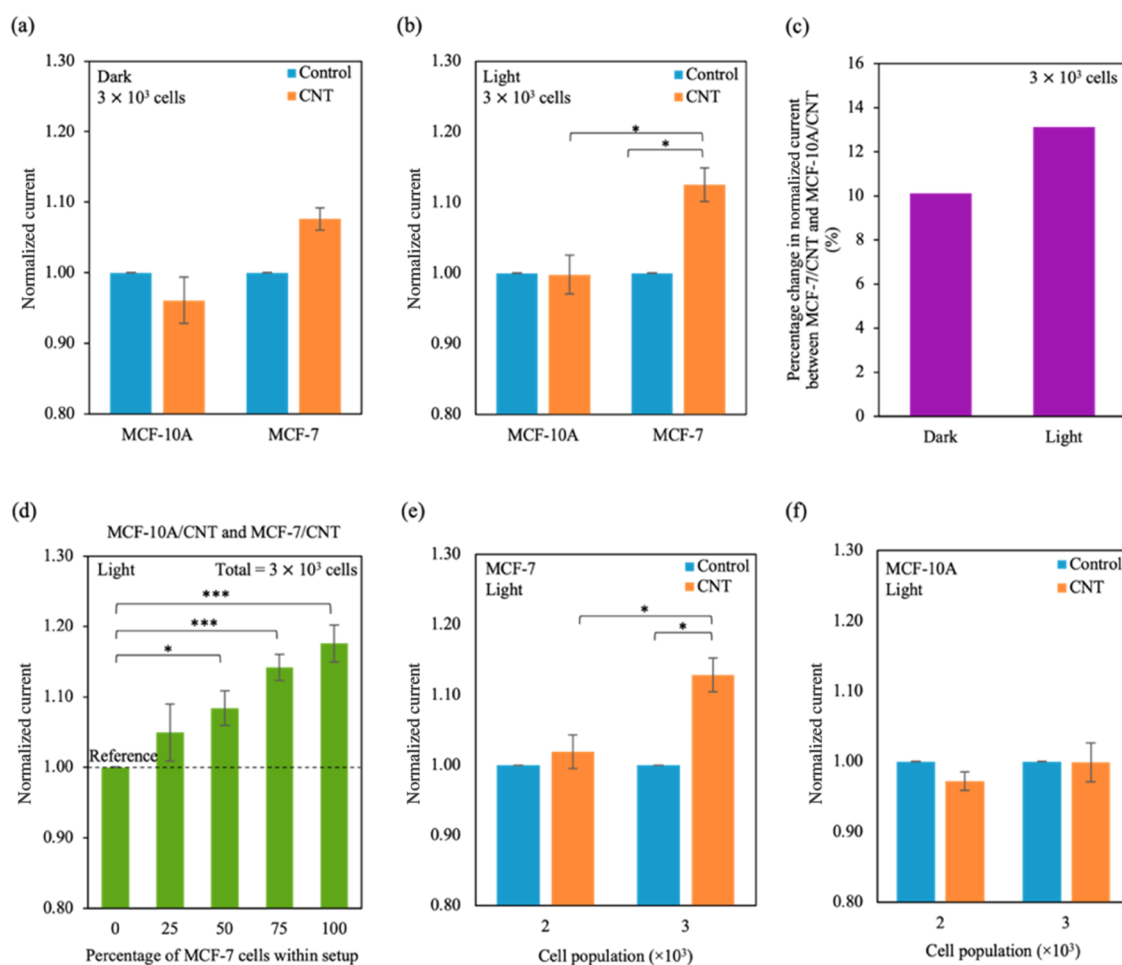
**Figure 2.** Sensing MCF-10A cells and MCF-7 cells using the CNT photo-assisted AC pulse sensor. (a, b) Normalized current varied for the different cell lines in (a) dark and (b) light conditions. Values were normalized with the respective controls (cells only), and the values for control were obtained experimentally. The raw data and normalized values can be found in Supporting Information Table S5. (c) Percentage difference in average normalized current between MCF-10A/CNT and MCF-7/CNT ($\Delta I_\%$) varies in dark and light conditions. The difference was calculated using eq 3, and values for average normalized currents were obtained from (a) and (b). (d) Normalized current was plotted for the percentage of MCF-7 cells within the heterogeneous population. Current output was normalized to MCF-10A cells alone ($n = 3 \times 10^3$ cells). The values for MCF-10A cells were obtained experimentally. Different percentages of MCF-7 cells (0, 25, 50, 75, 100%) were plated within total cell population ($n = 3 \times 10^3$ cells) in MCF-10A cell media. TThe black dotted line represents the reference normalized current (current output for MCF-10A cells only). (e, f) Plots of normalized current output with increasing (e) MCF-7 and (f) MCF-10A cell population. Values were normalized with the respective controls (cells only), and the values for controls were obtained experimentally. Data represent mean ± SEM, ($n = 6$ from 3 independent experiments). Significance was calculated using a Student's t-test and is presented as: * ($p < 0.05$) and *** ($p < 0.001$).

cytotoxicity of the material at a range of concentrations and incubation times. Cells were plated in a 96-well plate for ∼24 h prior to material treatment. Subsequently, cell viability was tested with a WST-1 assay and plates were measured at $\lambda = 450$ nm. Cytotoxicity was observed to be time- and concentration-dependent: increasing CNT concentration and the time of incubation from 24 to 48 h resulted in a decrease in cell viability, as seen in the literature.[2] This effect was more prominent in MCF-7 cells compared to MCF-10A cells (Figure 1e,f). The onset of the decrease in cell viability for MCF-10A cells occurs at the CNT concentration of ∼30 $\mu$g/mL. Based on the onset of the decrease in cell viability for MCF-10A cells and to achieve excellent electrical conduction, we chose to investigate the cytotoxicity of the MCF-10A cells and MCF-7 cells with ∼30 $\mu$g/mL CNT for ITO systems (Supporting Information Figure S2). The findings are similar to those in 96-well plates. Excellent cell viability was observed in the MCF-10A cells with ∼30 $\mu$g/mL CNT. The cell viability decreases with a change in cell type

from MCF-10A cells to MCF-7 cells. For subsequent electrical characterization, we chose to examine the MCF-10A/MCF-7 cells with ∼30 $\mu$g/mL CNT based on the cell viability conditions of MCF-10A cells in 96-well plates/ITO systems and electrical conduction considerations.

To understand the bioelectrical effects of the interaction between CNTs and the cells, we investigated the current obtained for the MCF-10A cells and MCF-7 cells with CNT (MCF-10A/CNT and MCF-7/CNT, respectively) after injecting bias voltage pulses in dark conditions. The current output for MCF-10A/CNT and MCF-7/CNT was normalized with control (cells with pulse, without CNT incubation). In Figure 2a, the normalized current obtained for MCF-7/CNT was ∼8% larger than the control. On the other hand, there was no significant difference observed for normalized current between control and MCF-10A/CNT.

The unique optical properties of CNTs can improve the current output: CNTs can be excited by light to enhance current
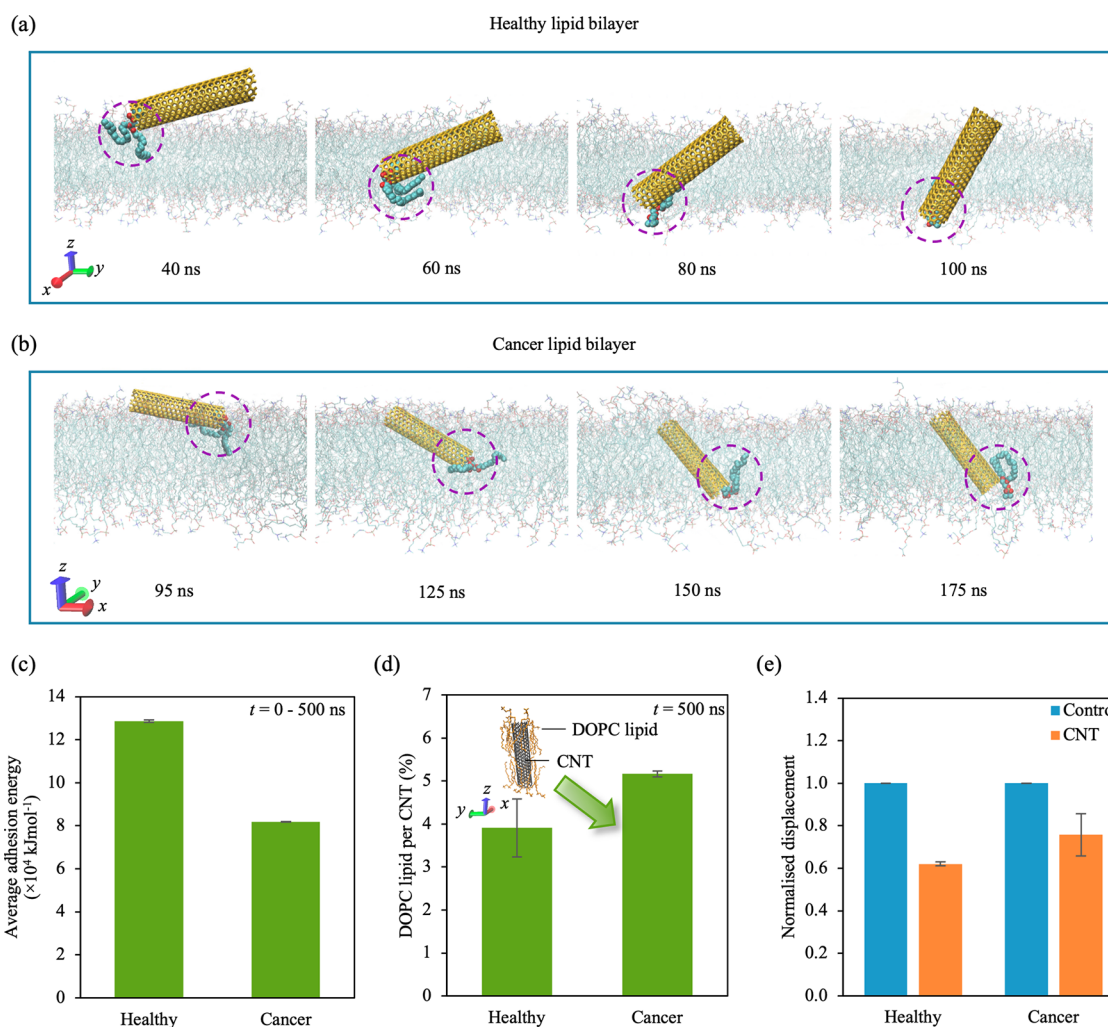
**Figure 3.** MD simulations of the healthy and cancer lipid bilayer systems with CNT. (a, b) Snapshots of the CNT spontaneously inserting into the (a) healthy and (b) cancer lipid bilayer over time. The headgroup of a DOPC lipid from the outer leaflet is shielded by the CNT during the insertion process. Both the CNT and the DOPC lipid molecule move into the hydrophobic core of the lipid bilayer. The DOPC lipid is represented as spheres, CNT is represented as sticks, and the other lipids are represented as lines for clarity. Color coding of atoms is as follows: O, red; N, navy blue; C, aqua; P, gold. Hydrogens and waters are omitted for clarity. (c) Average adhesion energy between the CNT and the healthy and cancer lipid bilayer systems. (d) Percentage of DOPC lipids interacting with CNTs within the two different systems. The cutoff distance was kept constant at 6 Å. The inset shows a snapshot of the CNT (black) interacting with DOPC lipids (orange) within the cancer lipid bilayer. Lipids positioned more than 6 Å away from the CNT were excluded for clarity. Hydrogens were omitted for clarity. (e) Self-diffusion coefficient for both lipid bilayer systems with CNTs (orange) normalized to control (blue). Simulation data are representative of two independent runs ($n = 2$).

and have been used as photodetectors. By exposing the system to light during electrical testing, we observed an increase of ~13% in the normalized current for MCF-7/CNT (Figure 2b). The difference in normalized current between the control and MCF-10A/CNT with light exposure was indistinguishable. Moreover, we plotted the difference between the average normalized currents for MCF-7/CNT to MCF-10A/CNT ($\Delta I_\%$) as a percentage using eq 3.

$$\Delta I_\% = \frac{I_{avg,MCF-7/CNT} - I_{avg,MCF10-A/CNT}}{I_{avg,MCF-10A/CNT}} \times 100\% \qquad (3)$$

where $I_{avg,MCF-7/CNT}$ is the average normalized current for MCF-7/CNT and $I_{avg,MCF-10A/CNT}$ is the average normalized current for MCF-10A/CNT. We demonstrate that light exposure produces a higher current contrast between MCF-7/CNT and MCF-10A/CNT (~13%) than dark conditions (~10%) (Figure 2c). Moreover, we observed a light intensity-dependant output. Current signals were normalized with MCF-7/CNT in dark

conditions, and they increased with increasing light intensity (Supporting Information Figure S3).

Furthermore, we propose that the CNT optoelectronic-pulse system is able to detect a small population of MCF-7 cells within a heterogeneous cell population. In a total population of $3 \times 10^3$ cells, different percentages of MCF-7 cells were plated with MCF-10A cells in MCF-10A cell media (see Experimental and Simulation Section and Supporting Information Table S1) and incubated with CNT for ~24 h. The current output was then measured and normalized to MCF-10A cells (0% of MCF-7, Figure 2d). As the percentage of MCF-7 cells increases within the heterogeneous cell population, we observed a corresponding increase in normalized current starting at 50% of MCF-7 (8, 14, and 17% for 50% of MCF-7, 75% of MCF-7, and 100% of MCF-7, respectively). The reference normalised current for the system was the current output for MCF-10A cells only. The detection limit for the system is ~$1.5 \times 10^3$ cells (50% of $3 \times 10^3$ cells), estimated by the smallest cell population with a normalized

current higher than the reference. Moreover, changes in normalized current were observed after increasing populations of MCF-7 cells from $2 \times 10^3$ to $3 \times 10^3$ cells but not for MCF-10A cells (Figure 2e,f). Thus, we demonstrate that the increase in current within the heterogeneous population is specific to the population of MCF-7 cells.

To estimate the selectivity for MCF-7 cells within the heterogeneous cell population, the current signals of potential interfering components (media and MCF-10A cells) were investigated. (Supporting Information Figure S4) The percentage change of current output after CNT addition ($\Delta x_{CNT,\%}$) was calculated using eq 4.

$$\Delta x_{CNT,\%} = \left| 1 - \frac{I_{sample/CNT}}{I_{sample}} \right| \times 100\% \qquad (4)$$

where $I_{sample}$ is the current output for samples (media only, control; MCF-10A cells; MCF-7 cells) and $I_{sample/CNT}$ is the current output for samples incubated with CNT. Both $I_{sample}$ and $I_{sample/CNT}$ were measured under light exposure. A substantial change in current signals upon CNT incubation was observed for MCF-7 cells ($\sim$9%). We observed negligible interference when control ($\sim$0.3%) or MCF-10A cells ($\sim$0.2%) were incubated with CNT, indicating that the CNT optoelectronic system is capable of selectively sensing changes in MCF-7 cells within a heterogeneous cell population (has an excellent anti-interference ability).

The MCF-7-specific change observed could be due to favorable interactions between the CNT and MCF-7 cell membrane. We propose that the system is able to detect MCF-7 cells with a limit of detection of $\sim$1.5 $\times 10^3$ cells within a heterogeneous cell population, lower than a baseline of $\sim$1 $\times 10^4$ cells[17] for existing electrical-based detection systems for a medium population of adhered cells (see Supporting Information Table S6). These findings show the potential of the CNT-based photo-assisted AC pulse system as a sensitive sensor for a small population of cancer cells within a heterogeneous cell population.

To investigate the basis of how CNTs can enhance system performance, all-atom MD simulations were performed to study the interaction between the healthy and cancer lipid bilayer systems with CNTs. As healthy cells transform into cancer cells, the asymmetry of the cell membrane is lost.[37,53] In healthy cells, a higher percentage of charged lipids reside in the inner leaflet, while the outer leaflet typically comprises neutral lipids. When asymmetry is lost, there is an even distribution of charged lipids between the inner and outer leaflet of a cancer cell membrane. Based on lipid compositions proposed by Klähn and Zacharias, we constructed a simple lipid bilayer comprising two lipid types: neutral dipalmitoylphosphatidylcholine (DOPC) and negatively charged dipalmitoylphosphatidylserine (DOPS) (Supporting Information Table S3).[37]

Trajectory snapshots of the (8,8) CNT ($l$ = 4.5 nm) interacting spontaneously with the healthy and cancer lipid membrane systems over time are shown in Supporting Information Figures S5a and S6a. The following observations are representative of both the two simulation runs, which are comparable. The CNT was initially positioned perpendicular to the lipid bilayer, about $\sim$2 nm away from the outer leaflet, before it spontaneously inserted itself into both the healthy and cancer lipid bilayers. Prior to membrane insertion, the CNT rested parallel to the top of the outer leaflet of the lipid bilayer. Additionally, before the insertion process, the headgroup of an outer leaflet DOPC lipid molecule inserted itself into one end of the CNT, thus shielding the charges (Figure 3a,b). The CNT and its associated DOPC lipid molecule then collectively moved into the hydrophobic core of the lipid bilayer. After the CNT was fully embedded within the hydrophobic tails of the lipid bilayer, the DOPC lipid head moved away from the CNT to face the solvent at the inner leaflet; as a result, the DOPC lipid molecule was inverted after CNT insertion. The CNT remained embedded within the hydrophobic core of the lipid bilayer due to favorable hydrophobic interactions.

The interaction between the CNT and the lipid bilayer systems was analyzed. Atom count, van der Waals (vdW) energy, and center of mass (CoM) distance were calculated over time and presented in Supporting Information Figures S5 and S6 for the healthy and cancer lipid bilayer systems, respectively. The average adhesion energy ($\Delta E$) between the CNT and the healthy and cancer lipid bilayer systems was calculated using eq 1 (see Experimental and Simulation Section). The average adhesion energy between the CNT and the healthy lipid bilayer was higher than that between the CNT and the cancer lipid bilayer, suggesting stronger interactions and an increased adhesion between the CNT and the healthy lipid bilayer (Figure 3c). The number of DOPC atoms interacting directly with the CNT (<6 Å) was calculated as a percentage using eq 2 (see Experimental and Simulation Section). Interestingly, a higher percentage of DOPC lipids within the cancer lipid bilayer ($\sim$5.17%) interacted with the embedded CNT compared to the healthy lipid bilayer ($\sim$3.91%) (Figure 3d). Interactions between CNT and DOPC lipids have been shown to disrupt the lipid bilayer by altering the orientation and mechanical properties of the lipids.[54,55] To further understand how the presence of the embedded CNT can affect the mechanical properties of the lipid, we calculated the mobility of the lipids, which can be estimated from the self-diffusion coefficient. Mean squared displacement was plotted as a function of time (Supporting Information Figure S7), and the self-diffusion coefficient was estimated from the slope of the curve. The self-diffusion coefficient for the healthy lipid bilayer with the embedded CNT decreased by approximately 40% compared to control, while a smaller decrease ($\sim$25%) was observed for the cancer lipid bilayer system (Figure 3e). While a decrease in mobility is expected due to the embedded CNT, the larger decrease for the lipids within the healthy lipid bilayer system could be associated with the higher adhesion energy between the CNT and the lipid bilayer system.

The substantially lower mobility of the lipids in combination with the higher adhesion energy with the CNT indicates that the healthy lipid bilayer becomes more rigid than the cancer lipid bilayer after CNT interaction. We suggest that cancer lipid bilayers undergo structural loosening as a result of CNT insertion. Hence, more CNTs are likely to be inserted into the cancer cell membrane than into the healthy cell membrane, enabling a larger current flow in cancer cells than in healthy cells when activated by an electrical-bias pulse (Figure 2a,b,e).

The proposed AC pulse light-assisted CNT system could be used to distinguish cancer cell lines from their healthy counterparts due to their differences in cell membrane compositions. Most cancer cells share similar mechanical characteristics; previous studies have shown that cancerous cells are less stiff compared to healthy cells. For example, Lekka et al. demonstrate that human bladder cancer cells were substantially less stiff compared to their healthy epithelial counterparts.[56] Similar results were reported for human ovarian

cancer cells and human breast cancer cells.[57,58] Thus, due to the differences in cell membrane compositions, we propose that the light-assisted CNT AC pulse system could be used to distinguish cancer cell lines from their healthy counterparts, as demonstrated in this work using MCF-7 cells and MCF-10A cells.

## DISCUSSION

Previously, cancer cells have been detected within heterogeneous cell populations using alternative methods such as traditional fluorescence imaging. Traditional probes based on CNTs typically require additional functionalization by fluorescent molecules (e.g., quantum dots or ligands) before material addition, as CNT is considered a substrate rather than an active constituent.[59] In addition, CNTs are generally suspended in surfactants during the functionalization process, such as sodium dodecylbenzene sulfate (SDS), which can be cytotoxic.[60] Recently, Raman imaging has been of interest to detect and monitor cancer cells. This method is unique, as Raman emissions have narrow spectra, allowing for the imaging of multiple Raman-active dyes with a low background noise.[61] Low dimensional nanomaterials such as CNTs are Raman active: they can be detected by traditional Raman spectroscopy methods via their unique vibrational frequencies.[62] While probes for this purpose can be designed with cancer cell specificity, these methods typically require additional time-consuming preparation steps and specialized equipment. CNTs can also exhibit photoluminescence under near-infrared (NIR) exposure due to their unique band gap structure, and have been used as optical probes.[63] However, to observe their photoluminescence, specialized laser setups may be required.[64,65] On the other hand, the CNT optoelectronic-pulse system does not require additional preparation methods or specialized equipment for detection. The method and setup are compact, low in cost, and easy to use, allowing the system to be connected to external circuitries and generate results quickly.

Another advantage of the proposed method is the detection performance; for instance, the time utilized for detecting the difference between healthy and cancer cells in the light-assisted CNT AC pulse system based on electrical conductance (~20 $\mu$s) can be shorter compared to traditional methods using pH and metabolic behavior. Conventional methods with fluorescent pH probes may require more than 24 h of incubation before cells can be visualized and the data can be collected.[66,67] Moreover, several limitations such as complex synthesis steps, low sensitivity, and poor reproducibility may also be faced by prototypical methods via fluorescent pH probes.[68] In addition, traditional methods based on hydrogen peroxide levels have been harnessed to detect cancer cells;[69−71] unlike healthy cells, cancer cells lack catalase and are unable to break down hydrogen peroxide. Experiments have demonstrated that the level of hydrogen peroxide released by cells increases when the cell types are changed from healthy cells to cancer cells.[69−71] However, the increased hydrogen peroxide level can be an indirect indicator for cancer cells. The level of hydrogen peroxide generated may also be influenced by the enzymes utilized and changes in pH,[72] Moreover, the proposed method is capable of distinguishing between healthy and cancer cells in real time without destroying the cells. Archetypal mass spectrometry methods can be utilized to differentiate between healthy and cancer cells based on their cell membrane lipid compositions, but these methods can be destructive and may require specific expertise.[73,74]

Electrical-based methods employing low dimensional materials have also been utilized to detect cancer cells. For example,

Abdolahad et al. demonstrated cell-selective impedance outputs for a single cell with frequencies ranging from 0 to 120 kHz using a CNT-based device.[14] While cells or biomolecules can be detected with high specificity, traditional electrical-based devices tend to detect single cells and appear to be single-use devices.[6] In this work, we were able to detect a heterogeneous population of adhered cells using the CNT optoelectronic-pulse system. Within a cell monolayer, cells are able to mimic the native tumor environment better than cells in suspension. In addition, cell−cell interconnects have proven to be important for electrical current studies.[18,19] The described system also has reusable components: the ITO electrodes on the glass substrate and cloning cylinders can be sterilized for future use,[75] reducing the cost of the system significantly.

CNT has demonstrated excellent biocompatibility and electrical properties and has been used to identify cancer cells from healthy cells using electrochemical methods. Traditional CNT-based sensing systems have demonstrated that MCF-7 cells are more sensitive to electrical stimulation than MCF-10A cells.[14] Moreover, similar CNT-based electrodes have been harnessed to determine the degree of metastasis for biopsied breast tissue samples.[32] However, CNTs used in these electrical detection methods are not in suspension but are fixed on the electrodes. It has been proposed that CNTs in solution can pass through the cell membrane via endocytosis or passive diffusion.[24] Furthermore, experimental studies demonstrate that CNTs aggregate within or close to the plasma membrane;[76,77] this could be due to the hydrophobic interactions observed between the CNT and the lipid tails (where the CNT embeds itself within the lipid bilayer).[78] We posit that MCF-7 cells have favorable CNT interactions that result in an MCF-7 cell-selective detection. Further research to investigate the mechanism of CNT uptake, such as functionalizing CNT with fluorescent probes, could provide a deeper understanding of the MCF-7 cell-CNT interaction.

Furthermore, we suggest that the proposed system could be utilized to detect early signs of tumorigenesis. In previous studies, combined nanomaterial electrical-based/nanomaterial-based systems have been harnessed to identify biomarkers or circulating tumor cells (CTCs) that can indicate early signs of cancer development.[79−82] For example, Yang et al. were able to electrochemically detect prostate-specific antigen (PSA) with a low detection limit using graphene sheets functionalized with quantum dots; PSA plays a crucial role in the early stages of prostate cancer development.[83] Using functionalized CNTs, Nima et al. were able to distinguish between healthy and cancer cells in suspension from Raman signals.[62] Thus, the proposed combination of CNT and AC-pulses can be similarly utilized to detect early signs of cancer development.

To further develop the CNT optoelectronic-pulse method for clinical relevance, it is important to detect cancer cells within a heterogeneous three-dimensional (3D) cell culture that can mimic tumor tissues found within the body. Designing detection systems for 3D cell cultures have been investigated.[84] For example, excised tissue samples can be placed into a measuring chamber with electrodes to connect the circuit.[85] Alternatively, tumor tissues extracted from patients can be cultured prior to detection.[86] Excised samples could be digested and cultured via traditional culture methods. Using an extracellular matrix (ECM) such as Matrigel, 3D cell cultures can be prepared to mimic native biological cues that are present in the body.[13,19] The subpopulation of cancer cells within the prepared 3D cell cultures can then be detected using the CNT optoelectronic-

pulse sensor (Supporting Information Figure S8). With the advancement of tissue engineering, 3D cell cultures can also be grown or bioprinted to integrate the cell culture with the system.[19,84]

One of the concerns of detecting cancer cells within a 3D cell culture is the electrical contribution of biological components found within the ECM; the ECM is present in tissues and organs and provides physical and biochemical cues for the cells.[19,84] Previous literature showed minimal effects on electrical output when cells were seeded on electrodes coated with ECM proteins (e.g., laminin, adhesion peptides, and other proteins).[87] Furthermore, real-time impedance responses were detected for lung cancer cells seeded on collagen-coated electrodes at different cell populations;[84] changes in impedance were recorded as cells proliferated over time. The study also showed that additional biological components found in complex ECM have little/no effect on current signals.[84] Further investigation and research on the CNT-based framework can develop a system to support ECM-based cell scaffolds with minimal effects on electrical output.

## CONCLUSIONS

In summary, we have demonstrated the efficiency and sensitivity of the CNT-based photo-assisted AC pulse sensor for the detection of MCF-7 cells. This method was able to enhance the bioelectrical signatures of MCF-7 cells by harnessing CNTs with AC pulse under light irradiation. Specifically, the sensor can detect $\sim 1.5 \times 10^3$ MCF-7 cells within an adherent heterogeneous population, an essential feature for identifying a small population of cancer cells. Additionally, all-atom MD simulations elucidate a structural loosening-facilitated increase in current. This system is compact, low in cost, and it has easy-to-use, reusable components that allow for easy implementation, improved user convenience, and high accessibility. Thus, the proposed sensor represents the first methodology reported using CNT-based photo-assisted AC pulse method for clinically relevant cancer cell detection and is an excellent building block for the development of lab-on-chip platforms.

## ASSOCIATED CONTENT

### ⓢ Supporting Information

The Supporting Information is available free of charge at https://pubs.acs.org/doi/10.1021/acsomega.2c00842.

> Experimental details describing the composition of heterogeneous cell populations (Table S1); parameters for modeling CNT (Table S2) and lipid bilayer composition (Table S3); tables provided also show significance for CNT cytotoxicity over time (Table S4); raw and normalized values for current output for MCF-10A cells and MCF-7 cells with and without CNT (Table S5) and limit of detection for other state-of-the-art electrical-based systems compared to this work (Table S6); additional figures provided show cell viability in heterogeneous cell media (Figure S1); cell growth and proliferation within the CNT-based optoelectronic-pulse setup (Figure S2); normalized current output as a function of light intensity (Figure S3) and percentage change of current output after CNT addition for MCF-10A cells and MCF-7 cells (Figure S4); further details of the MD simulations for both the healthy and cancer lipid bilayer model are also provided (Figures S5−S7); and schematic illustrations are provided to describe the

preparation of 3D cell cultures for detection with the CNT-based optoelectronic-pulse setup (Figure S8) (PDF)

## AUTHOR INFORMATION

### Corresponding Authors

**Natasa Bajalovic** − *Department of Science, Mathematics and Technology, Singapore University of Technology and Design, Singapore 487372, Singapore*; Email: natasa_bajalovic@sutd.edu.sg

**Desmond K. Loke** − *Department of Science, Mathematics and Technology, Singapore University of Technology and Design, Singapore 487372, Singapore; Office of Innovation, Changi General Hospital, Singapore 529889, Singapore*; ⓞ orcid.org/0000-0001-5799-6441; Email: desmond_loke@sutd.edu.sg

### Authors

**Sophia S. Y. Chan** − *Department of Science, Mathematics and Technology, Singapore University of Technology and Design, Singapore 487372, Singapore*; ⓞ orcid.org/0000-0001-6710-0469

**Denise Lee** − *Department of Science, Mathematics and Technology, Singapore University of Technology and Design, Singapore 487372, Singapore*; ⓞ orcid.org/0000-0001-5338-275X

**Maria Prisca Meivita** − *Department of Science, Mathematics and Technology, Singapore University of Technology and Design, Singapore 487372, Singapore*; ⓞ orcid.org/0000-0003-1518-0772

**Lunna Li** − *Department of Science, Mathematics and Technology, Singapore University of Technology and Design, Singapore 487372, Singapore; Thomas Young Centre and Department of Chemical Engineering, University College London, London WC1E 6BT, U.K.*

**Yaw Sing Tan** − *Bioinformatics Institute, Agency for Science, Technology and Research (A*STAR), Singapore 138671, Singapore*; ⓞ orcid.org/0000-0002-2522-9421

Complete contact information is available at:
https://pubs.acs.org/10.1021/acsomega.2c00842

### Notes

The authors declare no competing financial interest.
The data sets generated during and/or analyzed during the current study are available from the corresponding author on reasonable request.

## ■ REFERENCES

(1) Suleman, S.; Shukla, S. K.; Malhotra, N.; Bukkitgar, S. D.; Shetti, N. P.; Pilloton, R.; Narang, J.; Nee Tan, Y.; Aminbhavi, T. M. Point of Care Detection of COVID-19: Advancement in Biosensing and Diagnostic Methods. *Chem. Eng. J.* **2021**, *414*, No. 128759.

(2) Yang, D.; Liu, M.; Xu, J.; Yang, C.; Wang, X.; Lou, Y.; He, N.; Wang, Z. Carbon Nanosphere-Based Fluorescence Aptasensor for Targeted Detection of Breast Cancer Cell MCF-7. *Talanta* **2018**, *185*, 113−117.

(3) Zhang, J.; Shi, J.; Liu, W.; Zhang, K.; Zhao, H.; Zhang, H.; Zhang, Z. A Simple, Specific and "on-off" Type MUC1 Fluorescence Aptasensor Based on Exosomes for Detection of Breast Cancer. *Sens. Actuators, B* **2018**, *276*, 552−559.

(4) de Cremoux, P.; Extra, J. M.; Denis, M. G.; Pierga, J. Y.; Bourstyn, E.; Nos, C.; Clough, K. B.; Boudou, E.; Martin, E. C.; Müller, A.; Pouillart, P.; Magdélénat, H. Detection of MUC1-Expressing Mammary Carcinoma Cells in the Peripheral Blood of Breast Cancer Patients by Real-Time Polymerase Chain Reaction. *Clin. Cancer Res.* **2000**, *6*, 3117−3122.

(5) Berois, N.; Varangot, M.; Aizen, B.; Estrugo, R.; Zarantonelli, L.; Fernández, P.; Krygier, G.; Simonet, F.; Barrios, E.; Musé, I.; Osinaga, E. Molecular Detection of Cancer Cells in Bone Marrow and Peripheral Blood of Patients with Operable Breast Cancer. Comparison of CK19, MUC1 and CEA Using RT-PCR. *Eur. J. Cancer* **2000**, *36*, 717−723.

(6) Cheng, X.; Liu, Y. S.; Irimia, D.; Demirci, U.; Yang, L.; Zamir, L.; Rodríguez, W. R.; Toner, M.; Bashir, R. Cell Detection and Counting through Cell Lysate Impedance Spectroscopy in Microfluidic Devices. *Lab Chip* **2007**, *7*, 746−755.

(7) Friese, C. R.; Neville, B. A.; Edge, S. B.; Hassett, M. J.; Earle, C. C. Breast Biopsy Patterns and Outcomes in Surveillance, Epidemiology, and End Results—Medicare Data. *Cancer* **2009**, *115*, 716−724.

(8) Fajardo, L. L.; Pisano, E. D.; Caudry, D. J.; Gatsonis, C. A.; Berg, W. A.; Connolly, J.; Schnitt, S.; Page, D. L.; McNeil, B. J. Stereotactic and Sonographic Large-Core Biopsy of Nonpalpable Breast Lesions: Results of the Radiologic Diagnostic Oncology Group V Study1. *Acad. Radiol.* **2004**, *11*, 293−308.

(9) Williams, R. T.; Yao, K.; Stewart, A. K.; Winchester, D. J.; Turk, M.; Gorchow, A.; Jaskowiak, N.; Winchester, D. P. Needle Versus Excisional Biopsy for Noninvasive and Invasive Breast Cancer: Report from the National Cancer Data Base, 2003−2008. *Ann. Surg. Oncol.* **2011**, *18*, 3802−3810.

(10) Burbank, F. Stereotactic Breast Biopsy of Atypical Ductal Hyperplasia and Ductal Carcinoma in Situ Lesions: Improved Accuracy with Directional, Vacuum-Assisted Biopsy. *Radiology* **1997**, *202*, 843−847.

(11) Zalba, S.; ten Hagen, T. L. M. Cell Membrane Modulation as Adjuvant in Cancer Therapy. *Cancer Treat. Rev.* **2017**, *52*, 48−57.

(12) Schierbaum, N.; Rheinlaender, J.; Schäffer, T. E. Viscoelastic Properties of Normal and Cancerous Human Breast Cells Are Affected Differently by Contact to Adjacent Cells. *Acta Biomater.* **2017**, *55*, 239−248.

(13) Zhu, K.; Hum, N. R.; Reid, B.; Sun, Q.; Loots, G. G.; Zhao, M. Electric Fields at Breast Cancer and Cancer Cell Collective Galvanotaxis. *Sci. Rep.* **2020**, *10*, No. 8712.

(14) Abdolahad, M.; Janmaleki, M.; Taghinejad, M.; Taghnejad, H.; Salehi, F.; Mohajerzadeh, S. Single-Cell Resolution Diagnosis of Cancer Cells by Carbon Nanotube Electrical Spectroscopy. *Nanoscale* **2013**, *5*, 3421−3427.

(15) Marino, A. A.; Iliev, I. G.; Schwalke, M. A.; Gonzalez, E.; Marler, K. C.; Flanagan, C. A. Association between Cell Membrane Potential and Breast Cancer. *Tumor Biol.* **1994**, *15*, 82−89.

(16) Qiao, G.; Duan, W.; Chatwin, C.; Sinclair, A.; Wang, W. Electrical Properties of Breast Cancer Cells from Impedance Measurement of Cell Suspensions Related Content Single Cell Dielectric Spectroscopy. *J. Phys.: Conf. Ser.* **2010**, *224*, No. 012081.

(17) Chan, S. S. Y.; Lee, D.; Meivita, M. P.; Li, L.; Tan, Y. S.; Bajalovic, N.; Loke, D. K. Ultrasensitive two-dimensional material-based MCF-7 cancer cell sensor driven by perturbation processes. *Nanoscale Adv.* **2021**, *3*, 6974−6983.

(18) Li, L.; Hartley, R.; Reiss, B.; Sun, Y.; Pu, J.; Wu, D.; Lin, F.; Hoang, T.; Yamada, S.; Jiang, J.; Zhao, M. E-Cadherin Plays an Essential Role in Collective Directional Migration of Large Epithelial Sheets. *Cell. Mol. Life Sci.* **2012**, *69*, 2779−2789.

(19) Tandon, N.; Cannizzaro, C.; Chao, P.-H. G.; Maidhof, R.; Marsano, A.; Au, H.; Radisic, M.; Vunjak-Novakovic, G. Electrical Stimulation Systems for Cardiac Tissue Engineering. *Nat. Protoc.* **2009**, *4*, 155.

(20) Chakraborty, B.; Das, A.; Mandal, N.; Samanta, N.; Das, N.; Chaudhuri, C. R. Label Free, Electric Field Mediated Ultrasensitive Electrochemical Point-of-Care Device for CEA Detection. *Sci. Rep.* **2021**, *11*, No. 2962.

(21) Pumera, M.; Sánchez, S.; Ichinose, I.; Tang, J. Electrochemical Nanobiosensors. *Sens. Actuators, B* **2007**, *123*, 1195−1205.

(22) Loke, D. K.; Clausen, G. J.; Ohmura, J. F.; Chong, T. C.; Belcher, A. M. Biological-templating of a segregating binary alloy for nanowire-like phase-change materials and memory. *ACS Appl. Nano Mater.* **2018**, *1*, 6556−6562.

(23) Shah, K. A.; Shunaid Parvaiz, M.; Dar, G. N. Photocurrent in Single Walled Carbon Nanotubes. *Phys. Lett. A* **2019**, *383*, 2207−2212.

(24) Kostarelos, K.; Lacerda, L.; Pastorin, G.; Wu, W.; Wieckowski, S.; Luangsivilay, J.; Godefroy, S.; Pantarotto, D.; Briand, J.-P.; Muller, S.; Prato, M.; Bianco, A. Cellular Uptake of Functionalized Carbon Nanotubes Is Independent of Functional Group and Cell Type. *Nat. Nanotechnol.* **2007**, *2*, 108−113.

(25) Avouris, P.; Freitag, M.; Perebeinos, V. Carbon-Nanotube Photonics and Optoelectronics. *Nat. Photonics* **2008**, *2*, 341−350.

(26) Zhang, Y.; Iijima, S. Elastic Response of Carbon Nanotube Bundles to Visible Light. *Phys. Rev. Lett.* **1999**, *82*, 3472−3475.

(27) Barkelid, M.; Zwiller, V. Photocurrent Generation in Semi-conducting and Metallic Carbon Nanotubes. *Nat. Photonics* **2014**, *8*, 47−51.

(28) Hasobe, T.; Fukuzumi, S.; Kamat, P. V. Organized Assemblies of Single Wall Carbon Nanotubes and Porphyrin for Photochemical Solar Cells: Charge Injection from Excited Porphyrin into Single-Walled Carbon Nanotubes. *J. Phys. Chem. B* **2006**, *110*, 25477−25484.

(29) Şerban, C.; Cîmpean, M. A.; Raica, M. The Story of MCF-7 Breast Cancer Cell Line: 40 Years of Experience in Research. *Anticancer Res.* **2015**, *35*, 3147−3154.

(30) Lee, A. V.; Oesterreich, S.; Davidson, N. E. MCF-7 Cells— Changing the Course of Breast Cancer Research and Care for 45 Years. *J. Natl. Cancer Inst.* **2015**, *107*, No. djv073.

(31) Laurentius, L. B.; Owens, N. A.; Park, J.; Crawford, A. C.; Porter, M. D. Advantages and Limitations of Nanoparticle Labeling for Early Diagnosis of Infection. *Expert Rev. Mol. Diagn.* **2016**, *16*, 883−895.

(32) Zandi, A.; Gilani, A.; Abbasvandi, F.; Katebi, P.; Tafti, S. R.; Assadi, S.; Moghtaderi, H.; Parizi, M. S.; Saghafi, M.; Khayamian, M. A.; Davari sh, Z.; Hoseinpour, P.; Gity, M.; Sanati, H.; Abdolahad, M. Carbon Nanotube Based Dielectric Spectroscopy of Tumor Secretion; Electrochemical Lipidomics for Cancer Diagnosis. *Biosens. Bioelectron.* **2019**, *142*, No. 111566.

(33) Humphrey, W.; Dalke, A.; Schulten, K. VMD: Visual Molecular Dynamics. *J. Mol. Graph.* **1996**, *14*, 33−38.

(34) Benson, G. Editorial. *Nucleic Acids Res.* **2011**, *39*, W1−W2.

(35) Cornell, W. D.; Cieplak, P.; Bayly, C. I.; Kollman, P. A. Application of RESP Charges to Calculate Conformational Energies, Hydrogen Bond Energies, and Free Energies of Solvation. *J. Am. Chem. Soc.* **1993**, *115*, 9620−9631.

(36) Frisch, M. J.; Trucks, G. W.; Schlegel, H. B.; Scuseria, G. E.; Robb, M. A.; Cheeseman, J. R.; Scalmani, G.; Barone, V.; Petersson, G. A.; Nakatsuji, H.; Li, X.; Caricato, M.; Marenich, A. V.; Bloino, J.; Janesko, B. G.; Gomperts, R.; Mennucci, B.; Hratchian, H. P.; Ortiz, J. V.; Izmaylov, A. F.; Sonnenberg, J. L.; Williams-Young, D.; Ding, F.; Lipparini, F.; Egidi, F.; Goings, J.; Peng, B.; Petrone, A.; Henderson, T.; Ranasinghe, D.; Zakrzewski, V. G.; Gao, J.; Rega, N.; Zheng, G.; Liang, W.; Hada, M.; Ehara, M.; Toyota, K.; Fukuda, R.; Hasegawa, J.; Ishida, M.; Nakajima, T.; Honda, Y.; Kitao, O.; Nakai, H.; Vreven, T.; Throssell, K.; Montgomery, J. A. J.; Peralta, J. E.; Ogliaro, F.; Bearpark, M. J.; Heyd, J. J.; Brothers, E. N.; Kudin, K. N.; Staroverov, V. N.; Keith,

T. A.; Kobayashi, R.; Normand, J.; Raghavachari, K.; Rendell, A. P.; Burant, J. C.; Iyengar, S. S.; Tomasi, J.; Cossi, M.; Millam, J. M.; Klene, M.; Adamo, C.; Cammi, R.; Ochterski, J. W.; Martin, R. L.; Morokuma, K.; Farkas, O.; Foresman, J. B.; Fox, D. J. *Gaussian 16*, Revision C. 01. https://gaussian.com/citation/.

(37) Klähn, M.; Zacharias, M. Transformations in Plasma Membranes of Cancerous Cells and Resulting Consequences for Cation Insertion Studied with Molecular Dynamics. *Phys. Chem. Chem. Phys.* **2013**, *15*, 14427−14441.

(38) Jo, S.; Lim, J. B.; Klauda, J. B.; Im, W. CHARMM-GUI Membrane Builder for Mixed Bilayers and Its Application to Yeast Membranes. *Biophys. J.* **2009**, *97*, 50−58.

(39) Jämbeck, J. P. M.; Lyubartsev, A. P. An Extension and Further Validation of an All-Atomistic Force Field for Biological Membranes. *J. Chem. Theory Comput.* **2012**, *8*, 2938−2948.

(40) Chan, S. S. Y.; Tan, Y. S.; Wu, K.-X.; Cheung, C.; Loke, D. K. Ultra-High Signal Detection of Human Embryonic Stem Cells Driven by Two-Dimensional Materials. *ACS Appl. Bio Mater.* **2018**, *1*, 210−215.

(41) Li, L.; Belcher, A. M.; Loke, D. K. Simulating selective binding of a biological template to a nanoscale architecture: a core concept of a clamp-based binding-pocket-favored N-terminal-domain assembly. *Nanoscale* **2020**, *12*, 24214−24227.

(42) Abraham, M. J.; Murtola, T.; Schulz, R.; Páll, S.; Smith, J. C.; Hess, B.; Lindah, E. Gromacs: High Performance Molecular Simulations through Multi-Level Parallelism from Laptops to Supercomputers. *SoftwareX* **2015**, *1−2*, 19−25.

(43) Wang, J.; Wolf, R. M.; Caldwell, J. W.; Kollman, P. A.; Case, D. A. Development and Testing of a General Amber Force Field. *J. Comput. Chem.* **2004**, *25*, 1157−1174.

(44) Jorgensen, W. L.; Chandrasekhar, J.; Madura, J. D.; Impey, R. W.; Klein, M. L. Comparison of Simple Potential Functions for Simulating Liquid Water. *J. Chem. Phys.* **1983**, *79*, 926−935.

(45) Bussi, G.; Donadio, D.; Parrinello, M. Canonical Sampling through Velocity Rescaling. *J. Chem. Phys.* **2007**, *126*, No. 014101.

(46) Parrinello, M.; Rahman, A. Polymorphic Transitions in Single Crystals: A New Molecular Dynamics Method. *J. Appl. Phys.* **1981**, *52*, 7182−7190.

(47) Hoover, W. G. Canonical Dynamics: Equilibrium Phase-Space Distributions. *Phys. Rev. A* **1985**, *31*, 1695−1697.

(48) Nosé, S. A Unified Formulation of the Constant Temperature Molecular Dynamics Methods. *J. Chem. Phys.* **1984**, *81*, 511−519.

(49) Darden, T.; York, D.; Pedersen, L. Particle Mesh Ewald: An N·log(N) Method for Ewald Sums in Large Systems. *J. Chem. Phys.* **1993**, *98*, 10089−10092.

(50) Essmann, U.; Perera, L.; Berkowitz, M. L.; Darden, T.; Lee, H.; Pedersen, L. G. A Smooth Particle Mesh Ewald Method. *J. Chem. Phys.* **1995**, *103*, 8577−8593.

(51) Hess, B. P-LINCS: A Parallel Linear Constraint Solver for Molecular Simulation. *J. Chem. Theory Comput.* **2008**, *4*, 116−122.

(52) Skandani, A. A.; Zeineldin, R.; Al-Haik, M. Effect of Chirality and Length on the Penetrability of Single-Walled Carbon Nanotubes into Lipid Bilayer Cell Membranes. *Langmuir* **2012**, *28*, 7872−7879.

(53) Rivel, T.; Ramseyer, C.; Yesylevskyy, S. The Asymmetry of Plasma Membranes and Their Cholesterol Content Influence the Uptake of Cisplatin. *Sci. Rep.* **2019**, *9*, No. 5627.

(54) Parthasarathi, R.; Tummala, N. R.; Striolo, A. Embedded Single-Walled Carbon Nanotubes Locally Perturb Dopc Phospholipid Bilayers. *J. Phys. Chem. B* **2012**, *116*, 12769−12782.

(55) Garcia-Fandiño, R.; Piñeiro, Á.; Trick, J. L.; Sansom, M. S. P. Lipid Bilayer Membrane Perturbation by Embedded Nanopores: A Simulation Study. *ACS Nano* **2016**, *10*, 3693−3701.

(56) Lekka, M.; Laidler, P.; Gil, D.; Lekki, J.; Stachura, Z.; Hrynkiewicz, A. Z. Elasticity of Normal and Cancerous Human Bladder Cells Studied by Scanning Force Microscopy. *Eur. Biophys. J.* **1999**, *28*, 312−316.

(57) Xu, W.; Mezencev, R.; Kim, B.; Wang, L.; McDonald, J.; Sulchek, T. Cell Stiffness Is a Biomarker of the Metastatic Potential of Ovarian Cancer Cells. *PLoS One* **2012**, *7*, No. e46609.

(58) Wang, Y.; Xu, C.; Jiang, N.; Zheng, L.; Zeng, J.; Qiu, C.; Yang, H.; Xie, S. Quantitative Analysis of the Cell-Surface Roughness and Viscoelasticity for Breast Cancer Cells Discrimination Using Atomic Force Microscopy. *Scanning* **2016**, *38*, 558−563.

(59) Bhirde, A. A.; Patel, V.; Gavard, J.; Zhang, G.; Sousa, A. A.; Masedunskas, A.; Leapman, R. D.; Weigert, R.; Gutkind, J. S.; Rusling, J. F. Targeted Killing of Cancer Cells in Vivo and in Vitro with EGF-Directed Carbon Nanotube-Based Drug Delivery. *ACS Nano* **2009**, *3*, 307−316.

(60) Dong, L.; Joseph, K. L.; Witkowski, C. M.; Craig, M. M. Cytotoxicity of Single-Walled Carbon Nanotubes Suspended in Various Surfactants. *Nanotechnology* **2008**, *19*, No. 255702.

(61) Liu, Z.; Tabakman, S.; Sherlock, S.; Li, X.; Chen, Z.; Jiang, K.; Fan, S.; Dai, H. Multiplexed Five-Color Molecular Imaging of Cancer Cells and Tumor Tissues with Carbon Nanotube Raman Tags in the near-Infrared. *Nano Res.* **2010**, *3*, 222−233.

(62) Nima, Z. A.; Mahmood, M. W.; Karmakar, A.; Mustafa, T.; Bourdo, S.; Xu, Y.; Biris, A. S. Single-Walled Carbon Nanotubes as Specific Targeting and Raman Spectroscopic Agents for Detection and Discrimination of Single Human Breast Cancer Cells. *J. Biomed. Opt.* **2013**, *18*, No. 055003.

(63) Veetil, J. V.; Ye, K. Tailored Carbon Nanotubes for Tissue Engineering Applications. *Biotechnol. Prog.* **2009**, *25*, 709−721.

(64) Roxbury, D.; Jena, P. V.; Shamay, Y.; Horoszko, C. P.; Heller, D. A. Cell Membrane Proteins Modulate the Carbon Nanotube Optical Bandgap via Surface Charge Accumulation. *ACS Nano* **2016**, *10*, 499−506.

(65) Yudasaka, M.; Yomogida, Y.; Zhang, M.; Tanaka, T.; Nakahara, M.; Kobayashi, N.; Okamatsu-Ogura, Y.; Machida, K.; Ishihara, K.; Saeki, K.; Kataura, H. Near-Infrared Photoluminescent Carbon Nanotubes for Imaging of Brown Fat. *Sci. Rep.* **2017**, *7*, No. 44760.

(66) Urano, Y.; Asanuma, D.; Hama, Y.; Koyama, Y.; Barrett, T.; Kamiya, M.; Nagano, T.; Watanabe, T.; Hasegawa, A.; Choyke, P. L.; Kobayashi, H. Selective Molecular Imaging of Viable Cancer Cells with PH-Activatable Fluorescence Probes. *Nat. Med.* **2009**, *15*, 104−109.

(67) Lee, H.; Akers, W.; Bhushan, K.; Bloch, S.; Sudlow, G.; Tang, R.; Achilefu, S. Near-Infrared PH-Activatable Fluorescent Probes for Imaging Primary and Metastatic Breast Tumors. *Bioconjugate Chem.* **2011**, *22*, 777−784.

(68) Hou, H.; Zhao, Y.; Li, C.; Wang, M.; Xu, X.; Jin, Y. Single-Cell PH Imaging and Detection for PH Profiling and Label-Free Rapid Identification of Cancer-Cells. *Sci. Rep.* **2017**, *7*, No. 1759.

(69) Shu, Y.; Zhang, L.; Cai, H.; Yang, Y.; Zeng, J.; Ma, D.; Gao, Q. Hierarchical Mo2C@MoS2 Nanorods as Electrochemical Sensors for Highly Sensitive Detection of Hydrogen Peroxide and Cancer Cells. *Sens. Actuators, B* **2020**, *311*, No. 127863.

(70) Maji, S. K.; Sreejith, S.; Kumar Mandal, A.; Ma, X.; Zhao, Y. Immobilizing Gold Nanoparticles in Mesoporous Silica Covered Reduced Graphene Oxide: A Hybrid Material for Cancer Cell Detection through Hydrogen Peroxide Sensing. *ACS Appl. Mater. Interfaces* **2014**, *6*, 13648−13656.

(71) Zhu, L.; Zhang, Y.; Xu, P.; Wen, W.; Li, X.; Xu, J. PtW/MoS2 Hybrid Nanocomposite for Electrochemical Sensing of H2O2 Released from Living Cells. *Biosens. Bioelectron.* **2016**, *80*, 601−606.

(72) Asati, A.; Kaittanis, C.; Santra, S.; Perez, J. M. PH-Tunable Oxidase-like Activity of Cerium Oxide Nanoparticles Achieving Sensitive Fluorigenic Detection of Cancer Biomarkers at Neutral PH. *Anal. Chem.* **2011**, *83*, 2547−2553.

(73) Sorvina, A.; Bader, C. A.; Caporale, C.; Carter, E. A.; Johnson, I. R. D.; Parkinson-Lawrence, E. J.; Simpson, P. V.; Wright, P. J.; Stagni, S.; Lay, P. A.; Massi, M.; Brooks, D. A.; Plush, S. E. Lipid Profiles of Prostate Cancer Cells. *Oncotarget* **2018**, *9*, 35541−35552.

(74) Butler, L. M.; Perone, Y.; Dehairs, J.; Lupien, L. E.; de Laat, V.; Talebi, A.; Loda, M.; Kinlaw, W. B.; Swinnen, J. V. Lipids and Cancer: Emerging Roles in Pathogenesis, Diagnosis and Therapeutic Intervention. *Adv. Drug Delivery Rev.* **2020**, *159*, 245−293.

(75) Hu, R.; Su, X.; Liu, H.; Liu, Y.; Huo, M.-M.; Zhang, W. Recycled Indium Tin Oxide Transparent Conductive Electrode for Polymer Solar Cells Electronic Materials. *J. Mater. Sci.* **2020**, *55*, 11403−11410.

(76) Cheng, C.; Porter, A. E.; Muller, K.; Koziol, K.; Skepper, J. N.; Midgley, P.; Welland, M. Imaging Carbon Nanoparticles and Related Cytotoxicity. *J. Phys.: Conf. Ser.* **2009**, *151*, No. 012030.

(77) Porter, A. E.; Gass, M.; Muller, K.; Skepper, J. N.; Midgley, P. A.; Welland, M. Direct Imaging of Single-Walled Carbon Nanotubes in Cells. *Nat. Nanotechnol.* **2007**, *2*, 713−717.

(78) Lelimousin, M.; Sansom, M. S. P. Membrane Perturbation by Carbon Nanotube Insertion: Pathways to Internalization. *Small* **2013**, *9*, 3639−3646.

(79) Sharifi, M.; Avadi, M. R.; Attar, F.; Dashtestani, F.; Ghorchian, H.; Rezayat, S. M.; Saboury, A. A.; Falahati, M. Cancer Diagnosis Using Nanomaterials Based Electrochemical Nanobiosensors. *Biosens. Bioelectron.* **2019**, *126*, 773−784.

(80) Tabish, T. A.; Hayat, H.; Abbas, A.; Narayan, R. J. Graphene Quantum Dot−Based Electrochemical Biosensing for Early Cancer Detection. *Curr. Opin. Electrochem.* **2021**, *30*, No. 100786.

(81) Yoon, H. J.; Kim, T. H.; Zhang, Z.; Azizi, E.; Pham, T. M.; Paoletti, C.; Lin, J.; Ramnath, N.; Wicha, M. S.; Hayes, D. F.; Simeone, D. M.; Nagrath, S. Sensitive Capture of Circulating Tumour Cells by Functionalized Graphene Oxide Nanosheets. *Nat. Nanotechnol.* **2013**, *8*, 735−741.

(82) Huerta-Nuñez, L. F. E.; Gutierrez-Iglesias, G.; Martinez-Cuazitl, A.; Mata-Miranda, M. M.; Alvarez-Jiménez, V. D.; Sánchez-Monroy, V.; Golberg, A.; González-Díaz, C. A. A Biosensor Capable of Identifying Low Quantities of Breast Cancer Cells by Electrical Impedance Spectroscopy. *Sci. Rep.* **2019**, *9*, No. 6419.

(83) Yang, M.; Javadi, A.; Gong, S. Sensitive Electrochemical Immunosensor for the Detection of Cancer Biomarker Using Quantum Dot Functionalized Graphene Sheets as Labels. *Sens. Actuators, B* **2011**, *155*, 357−360.

(84) Chen, Y.; Zhang, J.; Wang, Y.; Zhang, L.; Julien, R.; Tang, K.; Balasubramanian, N. Real-Time Monitoring Approach: Assessment of Effects of Antibodies on the Adhesion of NCI-H460 Cancer Cells to the Extracellular Matrix. *Biosens. Bioelectron.* **2008**, *23*, 1390−1396.

(85) Blad, B.; Baldetorp, B. Impedance Spectra of Tumour Tissue in Comparison with Normal Tissue; a Possible Clinical Application for Electrical Impedance Tomography. *Physiol. Meas.* **1996**, *17*, A105.

(86) Shepherd, T. G.; Thériault, B. L.; Campbell, E. J.; Nachtigal, M. W. Primary Culture of Ovarian Surface Epithelial Cells and Ascites-Derived Ovarian Cancer Cells from Patients. *Nat. Protoc.* **2006**, *1*, 2643−2649.

(87) Jeong, H. C.; Choo, S. S.; Kim, K. T.; Hong, K. S.; Moon, S. H.; Cha, H. J.; Kim, T. H. Conductive Hybrid Matrigel Layer to Enhance Electrochemical Signals of Human Embryonic Stem Cells. *Sens. Actuators, B* **2017**, *242*, 224−230.